Trans Indian Inst Met (2017) 70(6):1477–1489
DOI 10.1007/s12666-016-0932-6

TECHNICAL PAPER

Initial Stage Oxidation and Surface Morphology of Modified 9Cr–1Mo Steel at High Temperatures in Air

M. Archana[1] · S. Ningshen[1] · C. Mallika[1] · U. Kamachi Mudali[1]

Received: 17 March 2016 / Accepted: 24 June 2016 / Published online: 9 July 2016

Abstract Modified 9Cr–1Mo steel was oxidized in air at 550 and 750 °C for 25, 100, 250 and 500 h and the oxide scales formed were analysed. The surface morphology and the chemical state of the oxide scales were evaluated using scanning electron microscopy (SEM) and X-ray photoelectron spectroscopy (XPS), respectively. The different exposure temperatures and time showed significant variations on the surface morphologies, the nature of oxide scale, and oxide constituents. The energy dispersive X-ray spectroscopic (EDS) analysis revealed the segregation of Mn at 750 °C even for short exposure time. Grazing incidence X-ray diffraction (GIXRD) patterns revealed the scales to be enriched with haematite and less intense magnetite peaks. Detailed XPS characterization indicated the presence of mixed oxides of iron (Fe), chromium (Cr) and manganese (Mn) in the oxide scales. The Fe–Cr spinel in the oxide scale offered resistance to oxidation of the steel, whereas Mn–Cr spinel was deleterious in nature as it promoted cracking and formation of blisters.

Keywords Modified 9Cr–1Mo steel · Initial oxidation · Surface morphology · Oxide scale · Mn–Cr spinel

1 Introduction

Modified (mod.) 9Cr–1Mo ferritic steel (niobium and vanadium added 9Cr–1Mo ferritic steel; referred to as Grade T91) is an important structural material used in high temperature steam/water environment due to its high resistance to water-induced stress corrosion cracking in caustic and chloride atmosphere, in addition to its high creep strength [1, 2]. The alloy derives its mechanical strength from solid solution strengthening with Nb and V containing precipitates, which contribute to creep strength [1, 3]. This material is normalized and tempered to achieve better mechanical properties. High thermal conductivity, low thermal expansion coefficient and high resistance to thermal fatigue have made T91 alloy a better replacement for low alloy steels used for the steam generator in power plants [4].

Modified 9Cr–1Mo steel has been chosen as the major structural material for the steam generator of prototype fast breeder reactor (PFBR) to be commissioned at Kalpakkam [1]. Selection of this material is primarily based on the combination of desirable mechanical properties such as creep, tensile and fatigue in addition to weldability, fabricability, microstructural stability, availability of engineering code and improved resistance to stress corrosion cracking in water/steam systems compared to austenitic stainless steels [1, 3]. However, one of the major limitations of this alloy is its susceptibility to oxidation and the consequent loss in wall thickness [2]. Hence, it is essential to understand the high temperature oxidation behavior of mod. 9Cr–1Mo steel. High temperature oxidation is a form of corrosion, in which the material degrades when exposed to oxygen containing atmosphere at higher temperatures. The sodium-cooled PFBR has been designed to operate at a temperature around 550 °C, where oxidation will be one of the major corrosive mechanisms. If oxidation is not controlled, it can lead to water or steam leak resulting in sodium–water interaction, and it should be avoided for safety reasons. The initial oxidation behavior of mod. 9Cr–1Mo steel has been studied extensively at 650 °C in ambient air [4]. The oxide growth rate is reported to be low

✉ S. Ningshen
ning@igcar.gov.in

[1] Corrosion Science and Technology Group, Indira Gandhi Centre for Atomic Research, Kalpakkam 603 102, India

in the presence of steam for 9Cr–1Mo steel due to the influence of Cr, resisting steam oxidation [5], and the oxide scale formed is a chemically delineated interface constituting binary and mixed ternary oxides. In a review on the oxidation of 9Cr–1Mo based steels in a steam environment, Fry et al. [6] reported that either V or W is detrimental to steam oxidation resistance. Laverde et al. [7] found that the oxidation of T91 ferritic steel in a steam saturated atmosphere under cyclic and isothermal conditions follows parabolic kinetics.

The mechanism of oxide scale formation on martensitic steels during steam oxidation and the micro structural characteristics of the oxide scale are found to vary with the chemical composition of the steel, oxidizing temperature and time of exposure [8, 9]. The kinetics of oxidation and the characteristics of the corrosion products depend upon the oxygen partial pressure of the aggressive environment. An increase in the temperature of oxidation will accelerate the oxidation process, which in turn increases the thickness of oxide scale, depending on the time of exposure. Development of initial oxide scale is controlled by temperature, pressure, the nature of corroding species and the composition of the material [3, 7]. As the oxide scale thickens, the flux of cations across the oxide layer decreases and reactions occurring within the oxide and the oxide-metal interface will become prominent [8]. It is reported that the presence of a small amount of chromium in the alloy leads to the formation of a chromium rich iron oxide; whereas, a higher concentration of Cr results in the formation of an iron–chromium spinel. The Fe–Cr spinel has been observed to be much denser and provides better oxidation resistance than the porous magnetite outer layer [6]. The complex layers formed on ferritic steels (with 9 wt% Cr) after exposure for 10000 h consists of a top outward growing Fe_3O_4 layer and an inward growing mixed oxide layer containing $(Fe,Cr)_3O_4$, FeO and Cr_2O_3 [9].

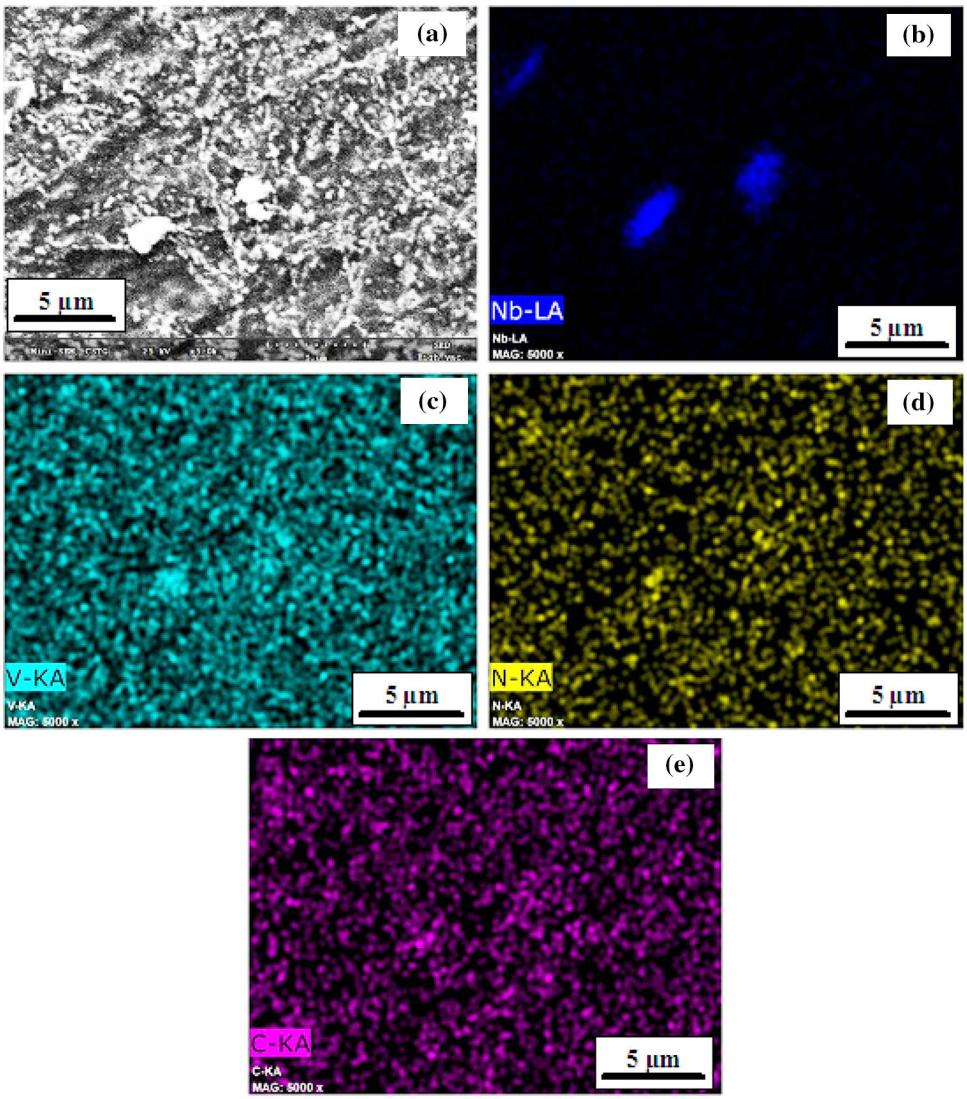

Fig. 1 **a** Surface morphology of the 'as received' modified 9Cr–1Mo steel, etched using Vilella's reagent for 1 min and **b–e** EDX maps showing the precipitates of MX (M = Nb, V and X = C, N) type

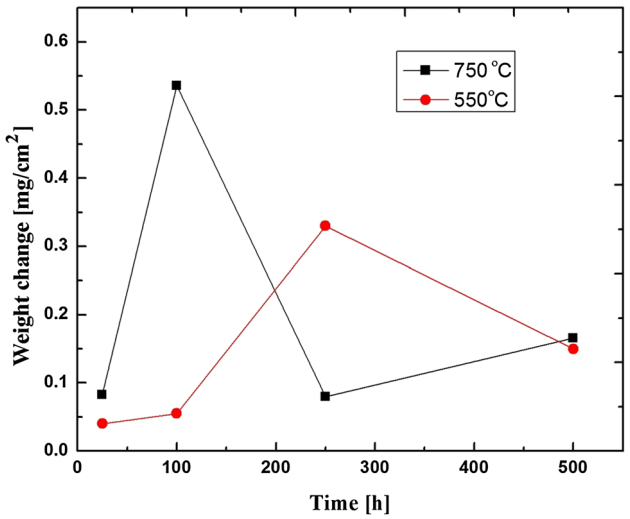

Fig. 2 Ex-situ weight change data with time at the temperatures 550 and 750 °C

In the present work, the oxidation behavior of mod. 9Cr–1Mo steel has been investigated at 550 and 750 °C in ambient atmospheric conditions for different exposure times ranging from 25 to 500 h, in order to understand the initial oxidation stages and the protective nature of the oxide layer. The morphology and chemical information on the oxide scales have been obtained using scanning electron microscopy (SEM), Grazing Incidence X-ray diffraction technique (GIXRD) and X-ray photoelectron spectroscopy (XPS).

2 Experimental Details

The chemical composition of mod. 9Cr–1Mo steel used in the present work was reported earlier [4]. Samples of dimensions, approximately 10 × 10 × 4 mm were sectioned from a plate of this steel. All the samples were mechanically ground up to 1200 grit using SiC emery sheets and cleaned in ethanol prior to oxidation studies. The polished samples were etched with Vilella's reagent (1 g picric acid and 5 ml concentrated HCl in 100 ml ethanol) for 1 min and the microstructures of the etched samples were characterized using SEM (Table top Mini-SEM, SEC Co Ltd, South Korea). Figure 1a represents the surface morphology of the 'as–received' mod. 9Cr–1Mo steel specimen, after etching.

The polished specimens were oxidised isothermally at the temperatures 550 and 750 °C in a resistance wound horizontal tubular furnace in atmospheric air for different exposure times ranging from 25 to 500 h. After each experiment, the samples were removed from the furnace and allowed to cool to room temperature to examine the oxide products. The weight changes in the oxidised samples were recorded to a precision of ±0.01 mg using an

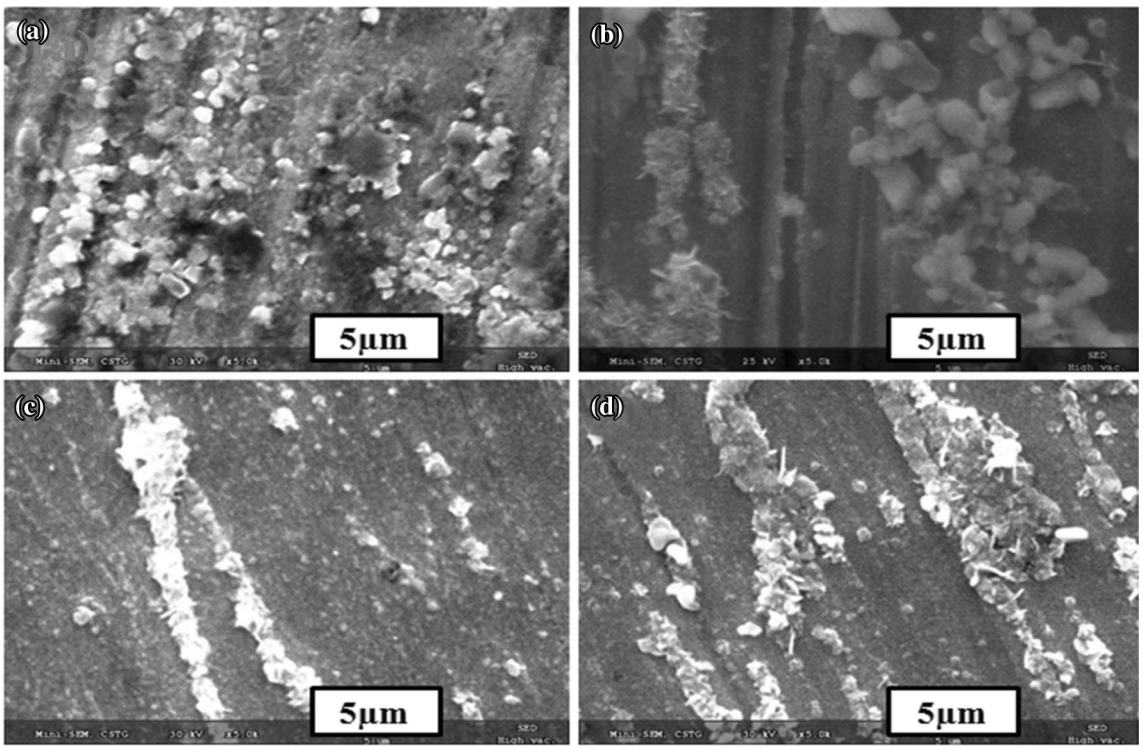

Fig. 3 SEM micrographs of mod. 9Cr–1Mo steel oxidized in ambient air at 550 °C at different durations: **a** 25 h; **b** 100 h; **c** 250 h and **d** 500 h

electronic balance. Surface morphology of the oxidized specimens were examined by SEM and elemental mapping was recorded using energy dispersive X-ray spectroscopy (EDX) to get qualitative information on the composition of the surface. Phase identification of the oxide film was carried out by INEL Equinox 2000 X-ray diffractometer (XRD) using Cu Kα radiation (wave length of Kα: 1.54 Å). The XPS (SPECS Surface Nano Analysis GmbH, Germany) analysis was performed in an ultra high vacuum chamber maintained at about 10^{-9} mbar and a PHOIBOS 150 spectrometer with monochromatic Al Kα radiation (1486.7 eV) was used for identifying the oxide products formed on the surface of the samples during oxidation. The XPS survey scans and high energy resolution spectra of the characteristic peaks of the elements Fe2P, Cr2P and Mn2P in the as-received and the oxidized samples were acquired.

3 Results and Discussion

3.1 Weight Change and Surface Morphology

The weight change in percentage was calculated for the mod. 9Cr–1Mo steel samples after oxidation as a function of exposure time at 550 and 750 °C in ambient atmosphere. Figure 2 shows the weight change during the course of oxidation. The weight of the samples increased with time initially at both the temperatures, and with increasing temperature the weight gain was more, indicating that the oxidation was temperature dependent. The initial increase in weight gain with time became insignificant for both the temperatures beyond 250 h of oxidation. This could be due to the local cracking of oxide film, fracture and void formation, thereby, giving rise to experimental scatter in the weight gain curves (Fig. 2) with increasing exposure time.

The morphology and structure of the oxide layers influenced the oxidation, if oxygen diffused along the grain boundaries and defects controlled the oxidation rate [10]. The micro-structure of etched mod. 9Cr–1Mo steel sample revealed that carbide particles were distributed uniformly in the matrix and the larger globular precipitates corresponded to V and Nb-enriched carbo nitrides. Elemental mapping using EDX spectroscopy attached with SEM upheld this observation. The average size of the carbides obtained from EDX analysis was in the range 1–2 micron and the distribution of the precipitates is shown in Fig. 1b–e. The SEM images of the oxides formed on the surface of the specimens at 550 and 750 °C for different exposure

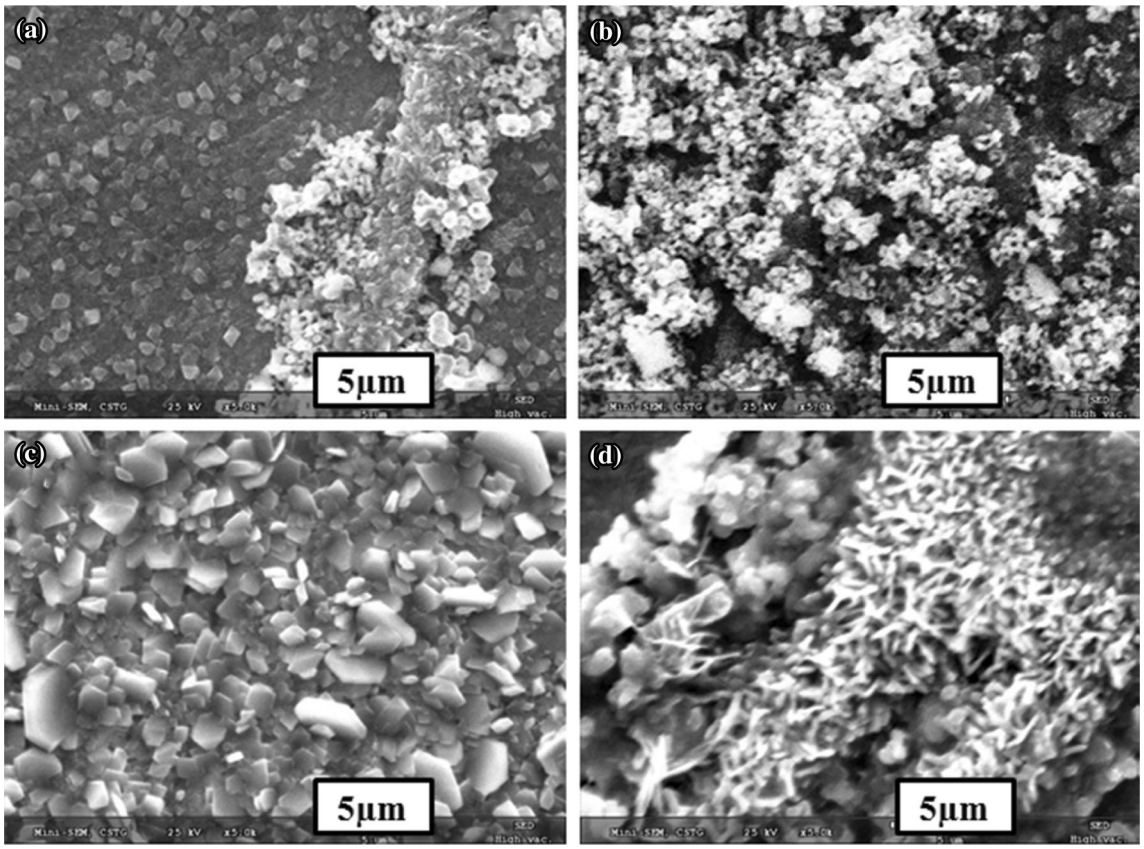

Fig. 4 SEM micrographs of mod. 9Cr–1Mo steel oxidized in ambient air at 750 °C: **a** 25 h; **b** 100 h; **c** 250 h and **d** 500 h

times are presented at a higher magnification in Figs. 3 and 4, respectively. The morphology of the oxide scales grown under different conditions differed significantly. The entire surface was covered with oxide globules and the size of the oxide globules was found to be increasing with increase in the exposure time. It was reported that the oxide growth took place within the scales while diffusional transport occurred by counter-current diffusion of metal and oxygen in the scale and as a result, the thickness of the scale increased and the growth of the scale was laterally along the surface [3, 5, 7]. The results of EDX analysis at different locations on the SEM micrographs for the samples oxidized at 550 and 750 °C are shown in Figs. 5 and 6, respectively. The composition profiles in Fig. 6 revealed the presence of O, Fe, Cr, Mn and C, implying the formation of a cluster of oxides constituted by Cr_2O_3 along with Fe–Cr and Mn–Cr mixed oxides. Fe was the major component and Cr and Mn were present in significant amounts; however, Mn was not found in the samples oxidized at 550 °C, as evidenced from Fig. 5. The concentration of Si in the oxide scale was below the detection limit of the instrument. The presence of minor alloying elements could have a significant effect on the initial oxidation and the nature of oxide scale. As the diffusion rate of manganese was high at 750 °C, it formed more stable oxides than iron and chromium, resulting in the amount of oxides of Mn as significant as that of Fe and Cr [11]. Figure 6 shows intense peaks corresponding to Mn

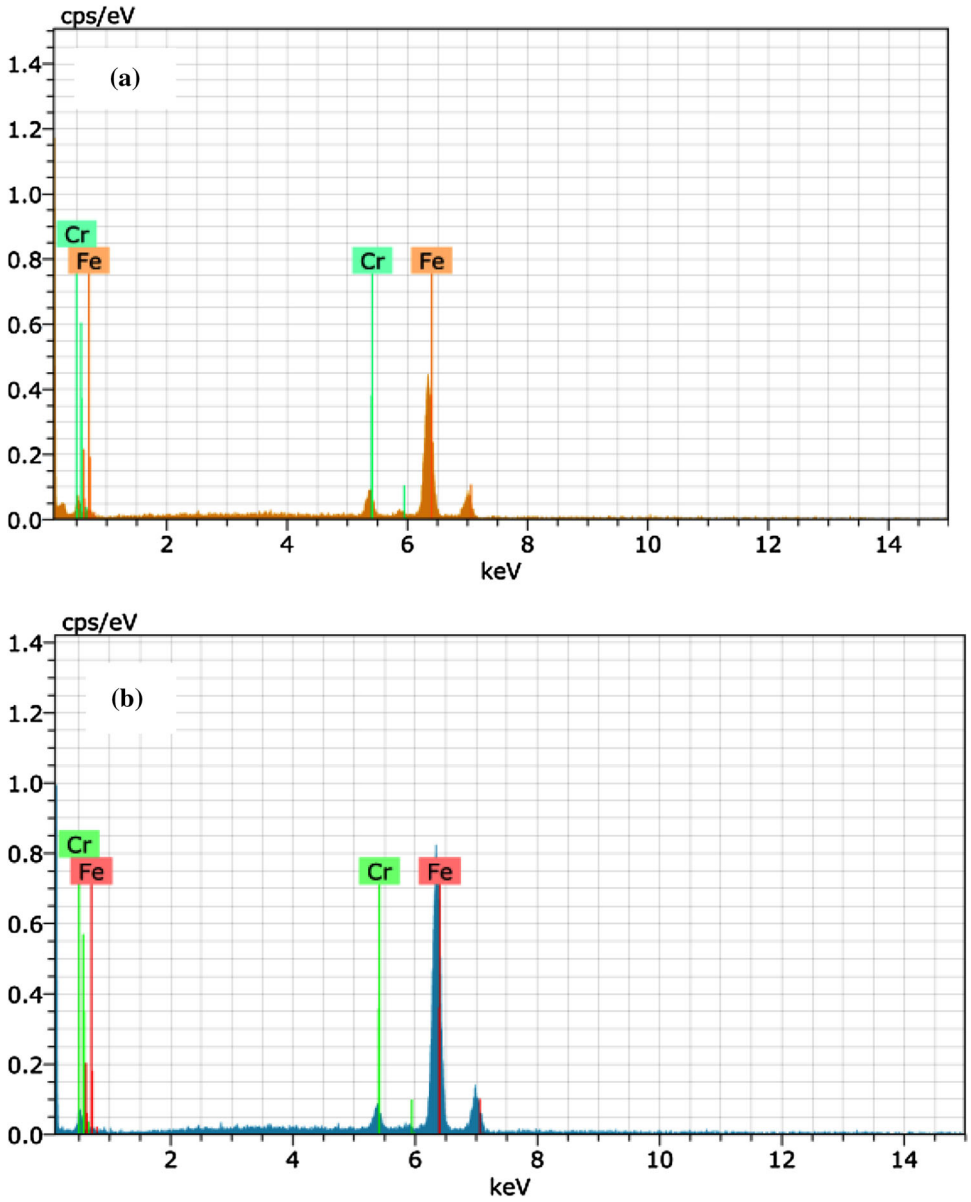

Fig. 5 EDX spectra of modified 9Cr–1Mo steel oxidized at 550 °C for different exposure times in ambient air: **a** 25 h, **b** 500 h

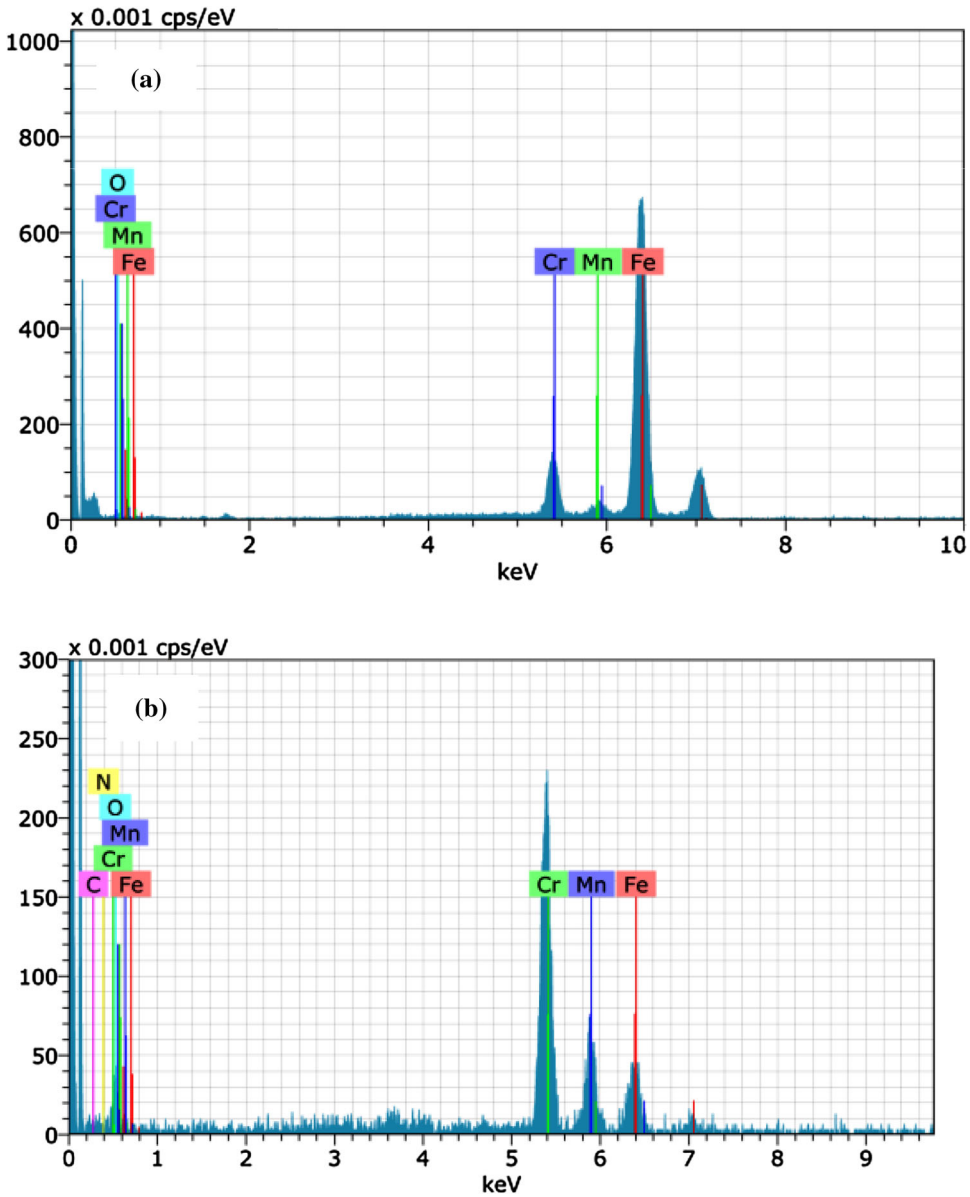

Fig. 6 EDX spectra of modified 9Cr–1Mo steel oxidized at 750 °C for different exposure times in ambient air: **a** 25 h, **b** 500 h

for those samples oxidized even for shorter exposure times, thereby confirming the diffusion of Mn. Viswanathan et al. [12] observed that the formation of oxide scales in 9–12 % Cr steels in water vapour environment was significantly affected by the presence of Mn in the temperature range 550–800 °C. Manganese-rich particles on the outer surface resulted in the initial oxidation, since the affinity of Mn for oxygen is greater than that for Cr and therefore, Mn ions diffused through chromia to the outer surface of the scale. However, the manganese content on the surface of the film was limited by the insignificant quantity of Mn present in the steel compared to the chromium content and thus, a spinel oxide was formed. As chromia did not act as a barrier for iron diffusion, iron diffused from the bulk into the oxide film [13].

3.2 Phase Analysis

The XRD pattern of the as-received mod. 9Cr–1Mo steel sample, reproduced in Fig. 7 is similar to that of ferrite (BCC Fe; JCPDS file No. 06-0696). The GIXRD patterns recorded for the samples subjected to oxidation at 550 and 750 °C for different durations are presented in Figs. 8 and 9, respectively. The various phases present on the surface of the oxidized samples were identified by comparing the diffraction spectra with the standard JCPDS patterns available for the corresponding phases. The peaks marked as α, β and χ corresponded to BCC Fe (JCPDS file No. 06-0696), hematite (JCPDS file No. 33-664) and magnetite (JCPDS file No. 19-0629), respectively. The presence of Fe (BCC) peaks in Figs. 8 and 9 revealed that the oxide layer

was thin and the metallic peaks were due to Fe from the bulk of the sample. The GIXRD analysis also indicated the formation of mainly iron oxides in all the samples. Lin et al. [14] reported that oxidation of ferritic steels resulted in the formation of a multi-layered scale on the surface comprising Fe_2O_3, Fe_3O_4 and FeO. The oxide scale formed in the present study consisted of Fe_2O_3 and Fe_3O_4 only, and the absence of FeO indicated the prevalence of reasonably higher oxygen potential. Though EDX spectra (Fig. 6) showed the presence of Cr and Mn peaks, phases corresponding to the oxides of Mn and Cr were absent in the GIXRD pattern shown in Fig. 9. As Fe was oxidized predominantly, the oxide scale on the surface consisted of mainly iron oxides and Cr was distributed below the iron oxide layer due to its inertness, compared to iron. The concentration of Cr and Mn in the steel were only 8.72 and 0.46 wt% respectively. Hence, the amount of these elements in the oxide scale might be below the detection limit of GIXRD technique, thereby indicating the absence of their corresponding oxides in the GIXRD patterns.

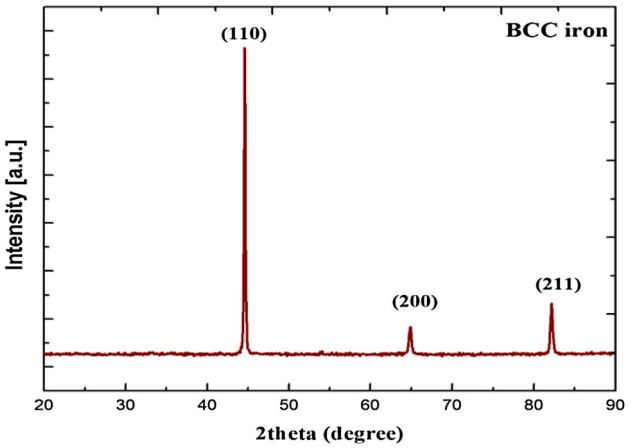

Fig. 7 GIXRD pattern of as-received mod. 9Cr–1Mo steel showing the presence of BCC iron

3.3 Characterisation of the Oxide Films by XPS

The XPS survey scan and the high-energy resolution spectra obtained for the surface and sub-surface zone of as-received mod. 9Cr–1Mo steel are presented in Fig. 10. The 2P spectra of Fe and Cr were collected and analyzed using XPSPEAK software. A Shirley type (non linear) background was used before deconvolution to eliminate the inelastically scattered electrons from the spectra and all the survey scans were analyzed to determine the stoichiometry of the compounds formed during oxidation. The fit made after background subtraction gave the lowest Chi square value. Binding energies of 711.1 and 577.0 eV confirmed the oxidation states of Fe and Cr on the surface of the as-received steel and the minor peaks appeared at 707.0 eV (Fe $2p_{3/2}$) and 574.3 eV (Cr $2p_{3/2}$) corresponded to their respective metallic states [5, 10]. Manganese was not detected in the survey spectra.

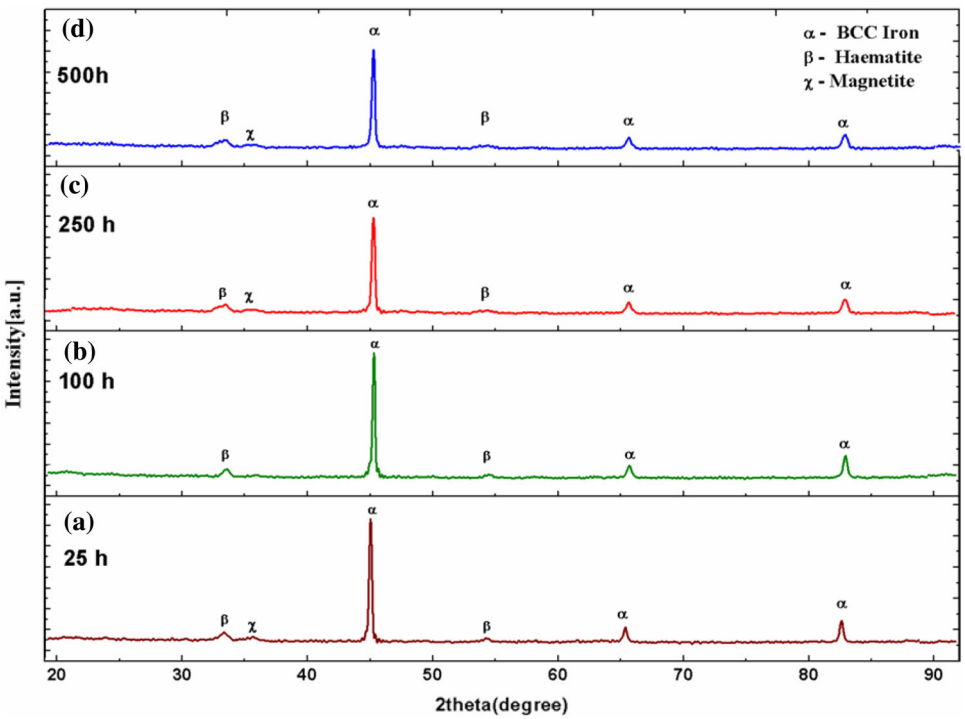

Fig. 8 GIXRD pattern of mod. 9Cr–1Mo steel, oxidized at 550 °C for different exposure time in ambient air: **a** 25 h, **b** 100 h, **c** 250 h and **d** 500 h

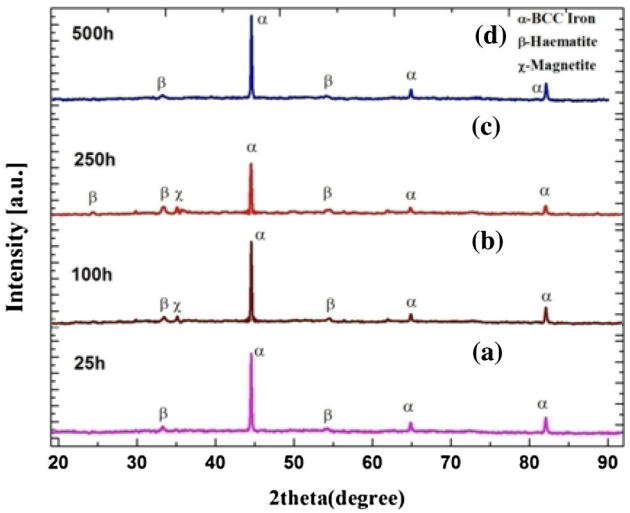

Fig. 9 GIXRD pattern of mod. 9Cr–1Mo steel, oxidized at 750 °C for different exposure time in ambient air: **a** 25 h, **b** 100 h, **c** 250 h and **d** 500 h

Figures 11 and 12 show the XPS spectra of the samples oxidized for 25 and 500 h respectively at 550 °C. The XPS spectra of the samples oxidized for 25 and 500 h at 750 °C are reproduced in Figs. 13 and 14, respectively. The deconvoluted peak position values, the number of component peaks, their width and separation for the samples oxidized for 25 and 500 h at 550 and 750 °C were listed in Tables 1 and 2, respectively. The binding energy values were observed to be in good agreement with the literature data [14–20]. The XPS results for the samples oxidized for 100 and 250 h at 550 and 750 °C were not shown since no significant change was observed in the oxidation patterns between 25 and 100 h as well as between 250 and 500 h duration. The O1s spectra for mod. 9Cr–1Mo steel oxidized at 750 °C for 25 h, represented in Fig. 15 were broad, indicating the presence of multiple compounds or oxidation states. The peak at 529.8 eV indicated the presence of metal oxides. The presence of metal oxides confirmed that the chemical state of oxygen was ionic. As the oxidation was carried out in ambient air, the water vapour content was negligible. The peak at 531.8 eV might correspond to metal carbonates due to carbon contamination.

Quantitative analysis of the XPS peaks of Fe 2p spectrum was complicated due to the spin–orbit splitting, multiple oxidation states and satellite structures [14–16]. The transition metals (Fe, Cr, Mn, etc.) existed in different oxidation states in both solid and liquid oxides. For instance, iron could be present as Fe^{2+} or Fe^{3+}, chromium as Cr^{2+}, Cr^{3+} or Cr^{6+} and manganese as Mn^{2+}, Mn^{3+} or Mn^{4+}. All orbital levels except s-level ($l = 0$) gave rise to the doublet with two possible states having different binding energies, which was known as the 'spin orbit coupling' and multiplet splitting arose when an atom contained unpaired electrons [15, 16]. Easy spectral curve fitting procedure adopted by Biesinger et al. [15, 16] was used in the present study to identify the chemical state of the transition metal (specifically Fe, Cr and Mn) that gave rise to multiplet splitting. The peak positions of Fe $2p_{1/2}$

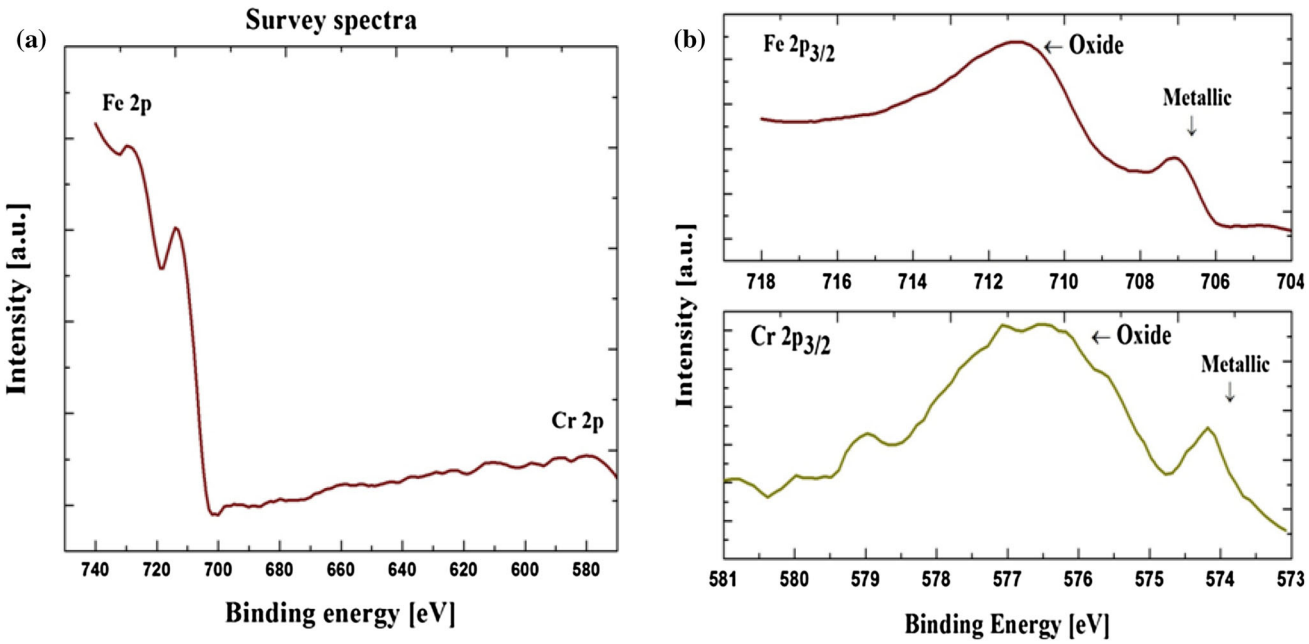

Fig. 10 The XPS survey and high-energy resolution spectra of as-received mod. 9Cr–1Mo steel showing the oxidized states of Fe and Cr, as native oxides on the surface

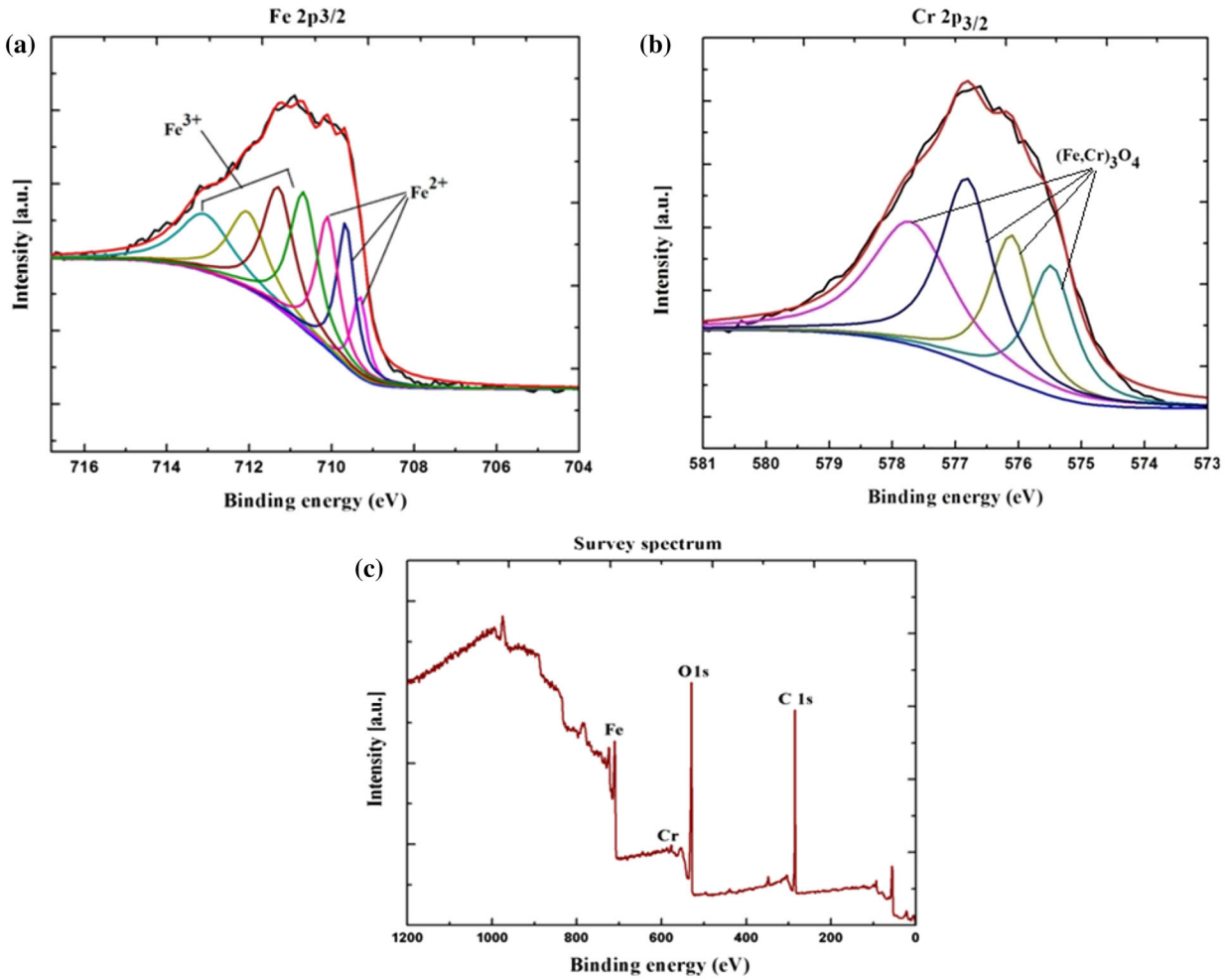

Fig. 11 XPS high resolution spectra of modified 9Cr–1Mo steel oxidized at 550 °C for 25 h: **a** Fe $2p_{3/2}$ spectrum, **b** Cr $2p_{3/2}$ spectrum and **c** XPS survey spectrum

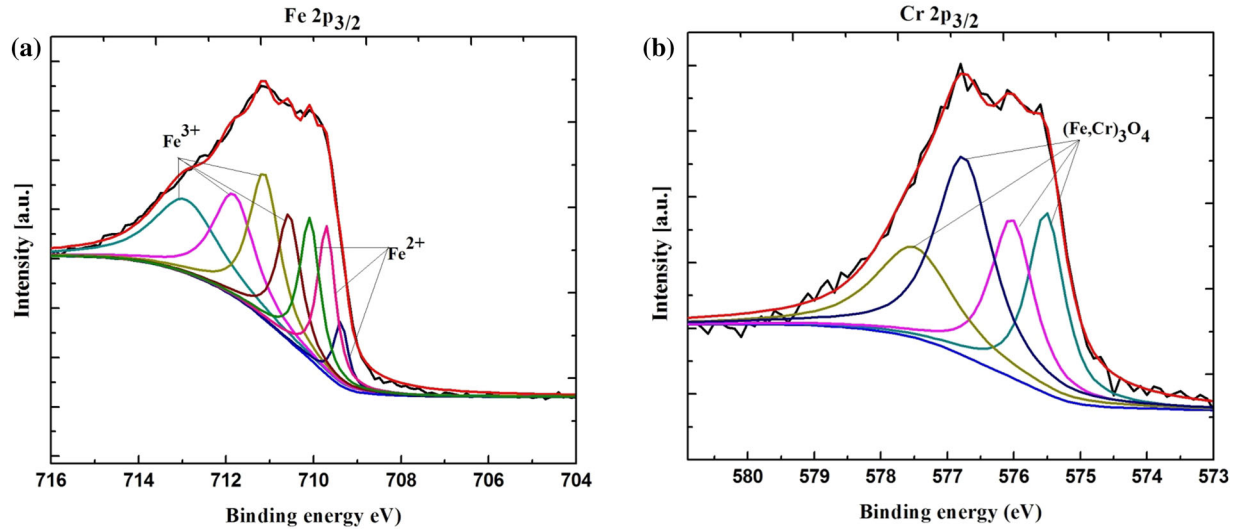

Fig. 12 XPS high resolution spectra of modified 9Cr–1Mo steel oxidized at 550 °C for 500 h: **a** Fe $2p_{3/2}$ spectrum, **b** Cr $2p_{3/2}$ spectrum

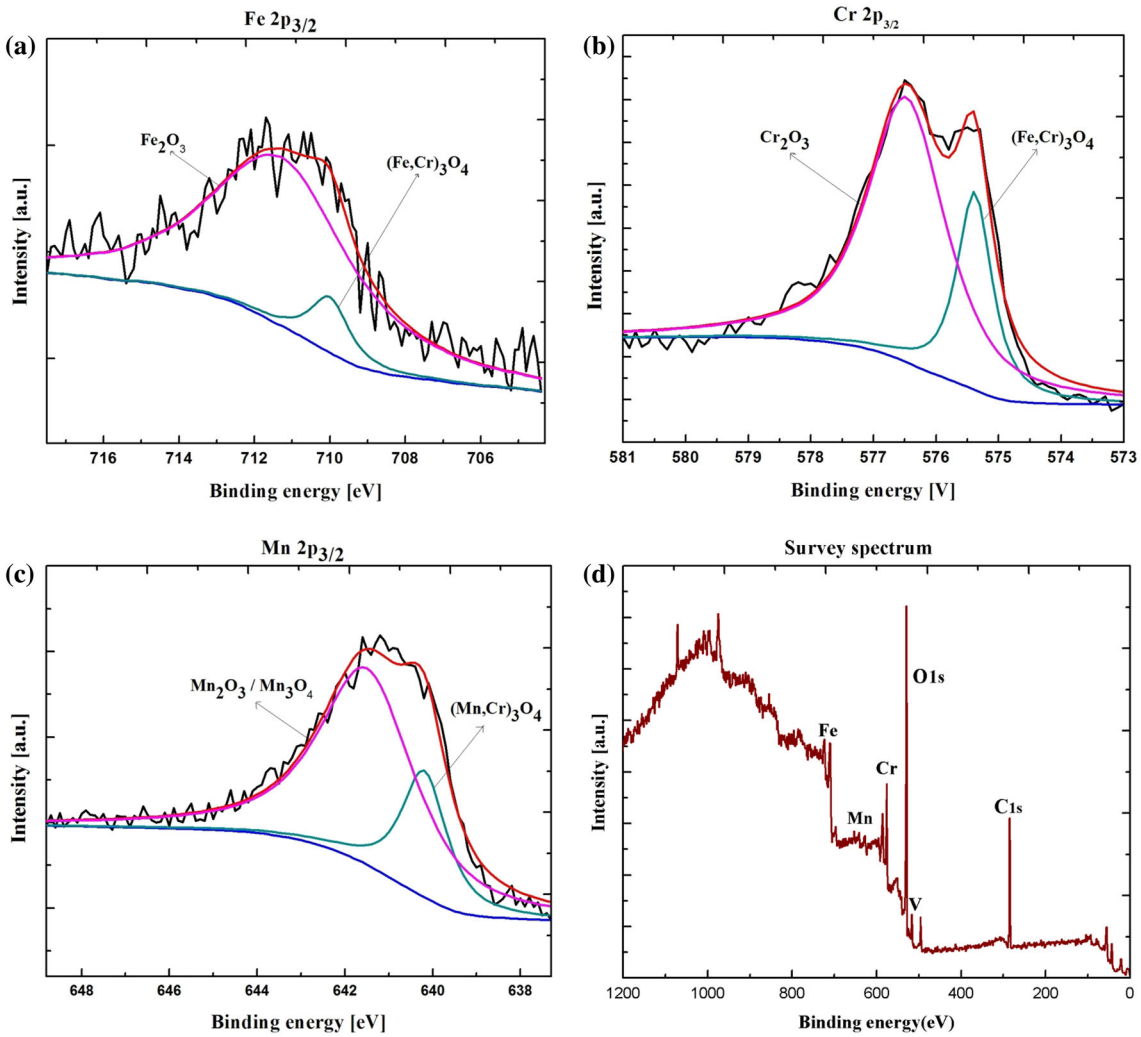

Fig. 13 XPS spectra of modified 9Cr–1Mo steel oxidized at 750 °C for 25 h: **a** Fe $2p_{3/2}$ spectrum, **b** Cr $2p_{3/2}$ spectrum, **c** Mn $2p_{3/2}$ spectrum and **d** XPS survey spectrum

and Fe $2p_{3/2}$ depended on the ionic states of Fe, and was the same with Cr and Mn. The positions of the satellite peaks for Fe $2p_{1/2}$ and Fe $2p_{3/2}$ were also sensitive to the oxidation states and those peaks were used for qualitatively determining the ionic states of iron. The $2p_{3/2}$ spectra of Fe (oxidized for 100, 250 and 500 h) could not be deconvoluted with a single symmetric Gaussian/Lorentzian peak due to its multiple oxidation states. The asymmetric shape of the peak might be attributed to the two oxidation states Fe^{2+} and Fe^{3+} and a set of two peaks were used for fitting the spectral data. Peak position values of Fe $2p_{3/2}$ spectra listed in Tables 1 and 2 represented the oxidized form. The higher Cr content resulted in the formation of Fe–Cr spinel. Table 1 revealed multiplet splitting of Fe in the samples oxidized at 550 °C, whereas the effect of multiplet interaction was less pronounced in the samples oxidized at 750 °C [17]. The Fe^{3+} state had the outer shell configuration as $3p^6 3d^5$ and the broader envelope could be attributed to the multiplet interaction. The binding energies 711 and 709 eV were characteristic of Fe^{3+} and Fe^{2+} respectively [18]. Based on XPS results, Machet et al. [19] reported the presence of Fe_3O_4 and $(Fe,Cr)_3O_4$ spinel structured compounds. As ferritic steel contained sufficient amount of Cr, oxides of chromium would be formed and since Cr dissolved in magnetite to form Fe–Cr spinels, better oxidation resistance was offered by Cr than simple iron oxides in which the binding energy fell between FeO and Fe_2O_3 [20].

In the high-resolution spectra of Cr $2p_{3/2}$, the peak envelope was fitted with multiplet splitting peaks. Multiplet splitting arose when an atom had unpaired electrons. When a core electron vacancy was made by photo ionization, there could be angular momentum coupling of the unpaired electron in the core with that of the outer shell, thereby

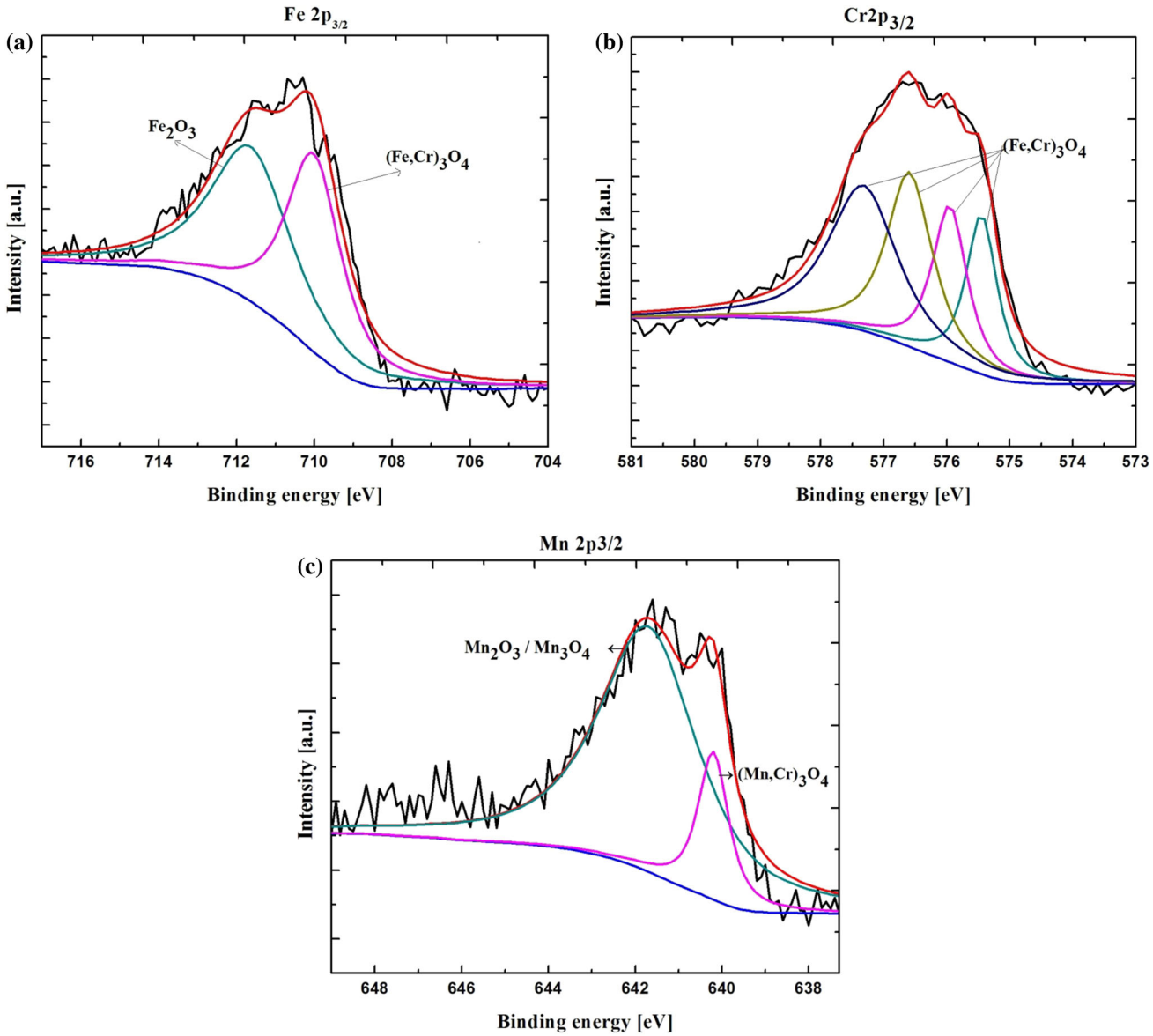

Fig. 14 XPS results for modified 9Cr–1Mo steel oxidized at 750 °C for 500 h: **a** Fe $2p_{3/2}$ spectrum, **b** Cr $2p_{3/2}$ spectrum and **c** Mn $2p_{3/2}$ spectrum

creating a number of final states which were manifested in the XPS spectra [17]. As Cr^{3+} state had the outer shell configuration as $3p^6 3d^3$, the broader envelope could be attributed to the free ion multiplet splitting of Cr^{3+}, which was consistent with the reported results [13, 15]. The Cr 2p spectrum corresponded to the multiplet structure of Cr_2O_3. The overall peak position and spectral shape of $FeCr_2O_4$ and Cr_2O_3 were observed to be overlapped.

The emergence of Mn was detected in the wide scan spectra of the samples oxidized at 750 °C along with Fe 2p and Cr 2p signals, whereas it was not detected in those samples oxidized at 550 °C. Segregation and oxidation of Mn could modify the activity of Fe and Cr at the oxide/alloy interface. The XPS data confirmed the formation of Mn–Cr spinel, along with the binary oxides of manganese. The higher binding energy component was attributed to the formation of binary Mn-oxides (Mn_2O_3/Mn_3O_4) and the lower binding energy component was assigned to the formation of ternary (Mn, $Cr)_3O_4$ [20]. The presence of Mn adversely affected the oxidation behavior as the diffusion rates were faster in the spinel, compared to the Cr_2O_3 layer, besides promoting blistering and cracking [21].

4 Conclusions

The initial stage of oxidation of mod. 9Cr–1Mo steel was investigated at 550 and 750 °C in ambient air for the exposure time ranging from 25 to 500 h. The weight gain

Table 1 XPS peak positions of mod. 9Cr–1Mo steel oxidized at 550 °C for different time periods [15, 16, 18]

Duration of oxidation (h)	Binding energy (eV)					
	Fe			Cr		
	Peak (eV)	FWHM	BE (eV) separation	Peak (eV)	FWHM	BE (eV) separation
25	709.3	0.4	0.3	575.5	0.8	0.6
	709.6	0.5	0.5	576.1	0.8	0.7
	710.1	0.6	0.6	576.8	1	0.9
	710.7	0.8	0.6	577.7	1.6	
	711.3	0.9	0.7			
	712	1.1	1.1			
	713.1	1.5				
500	709.4	0.4	0.3	575.5	0.7	0.5
	709.7	0.5	0.4	576	0.8	0.7
	710.1	0.6	0.4	576.7	1	0.8
	710.5	0.6	0.6	577.5	1.4	
	711.1	0.8	0.7			
	711.8	1.2	1.1			
	712.9	1.8				

Table 2 XPS peak positions of mod. 9Cr–1Mo steel oxidized at 750 °C for different durations [15, 16, 18]

Oxidation time (h)	Binding energy values (eV)							
	Fe			Cr			Mn	
	Peak (eV)	FWHM	BE (eV) separation	Peak (eV)	FWHM	BE separation (eV)	Peak (eV)	FWHM
25	712.3	3	1.9	575.4	0.7	1.1	640.2	1.3
	710.4	1.7		576.5	1.5		641.5	
500	711.6	2.4	1.6	575.4	0.6	0.5	641.6	2.7
	710	1.7		575.9	0.7	0.7	640.2	0.8
				576.6	0.9	0.7		
				577.3	1.3			

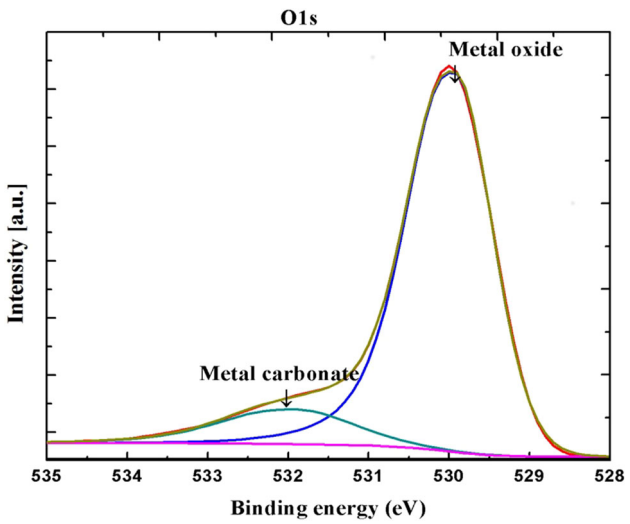

Fig. 15 The typical O 1s spectrum for modified 9Cr–1Mo steel oxidized at 750 °C for 25 h indicating the presence of metal oxides

during initial oxidation revealed that the oxidation was time and temperature dependent. The morphology of the oxide scales grown under different durations at the isothermal temperature differed significantly. The SEM images indicated that nucleation and growth of oxide scale occurred with an increase in exposure time. Segregation and oxidation of Mn were visible in all the oxidized samples even for the lowest exposure time at 750 °C, whereas they were absent in the samples oxidized at 550 °C. The EDX elemental maps indicated the formation of a cluster of oxides constituted by Cr_2O_3 along with Fe–Cr and Mn–Cr mixed oxides, for the samples oxidized at 750 °C. The XPS analysis revealed the presence of oxidized Fe and Cr species. High-resolution spectra of chromium showed multiplet splitting. The constitution of the scales formed on the surface upon oxidation was binary oxides of Fe, Cr and Mn and mixed Fe–Cr and Mn–Cr spinels. The Fe–Cr spinel in the oxide scale provided a protective film, whereas Mn–Cr

spinel was non-protective and resulted in the cracking of oxide layer.

Acknowledgments The authors gratefully acknowledge Mr. Nanda Gopala Krishna, Corrosion Science and Technology Group, IGCAR for his help in obtaining XPS data.

References

1. Raj B, Mannan S L, Vasudeva Rao P R, Mathew M D, *Sadhana* **27** (2002) 527.
2. Rajendran Pillai S, Dayal R K, *Oxid Met* **69** (2008) 131.
3. Faulkner R G, Abe F, Kern T U, Viswanathan R, *Grain Boundaries in Creep Resistant Steels*, CRC Press, Woodhead Publishing, Cambridge, England (2008), p 329.
4. Srinivasan S, Mallika C, Krishna NG, Thinakaran C, Jayakumar T, Kamachi Mudali U, *Corros Sci* **79** (2014) 59.
5. Osgerby S, Fry T, *Mater Res* **7** (2004) 141.
6. Fry T, Osgerby S, Wright M *Oxidation of Alloys in Steam Environments—A Review*, NPL Report, MATC(A)90, Sept. (2002).
7. Laverde D, Gomez-Acebo T, Castro F, *Corros Sci* **46** (2004) 613.
8. Sequeria C A C, Chen Y, Santos D M F, Song X, *Corros Prot Mater* **27** (2008), 114.
9. Agüero A, Gonzáleza V, Mayr P, Spiradek-Hahn K, *Mater Chem Phys* **141** (2013) 432.
10. Ampornrat P, Was G S, *J Nucl Mater* **371** (2007) 1.
11. Tariq Malik M, Bergner D, *Crystal Res. Technol* **23** (1988) 1503.
12. Viswanathan R, Sarver J, Tanzosh J M *J Mater Eng Perform* **15** (2006) 255.
13. de Fatima Salgado M, Sabionia A C S, Huntz A, Rossi E H, *Mater Res* **11** (2008) 227.
14. Lin T -C, Seshadri G, Kelber J A, *Appl Surf Sci* **119** (1997) 83.
15. BiesingerM C, Payne B P, Grosvenor A P, Lau L W M, Gerson A R, Smart R S C, *Appl Surf Sci* **257** (2011) 2717.
16. Biesinger M C, Lau L W M, Gerson A R, *Appl Surf Sci* **257** (2010) 887.
17. Grosvenor A P, Kobe B A, Biesinger M C, McIntyre N S, *Surf Interface Anal* **36** (2004) 1564.
18. Aronniemi M, Lahtinen J, Hautojarvi P, *Surf Interface Anal* **36** (2004) 1004.
19. Machet A, Galtayries A, Marcus P, Combrade P, Jolivet P, Scott P, *Surf Interface Anal* **34** (2002) 197.
20. Moulder J F, Stickle W F, Sobol P E, Bomben K D, *Handbook of X-ray Photoelectron Spectroscopy*, Perkin–Elmer Corp., Eden Prairie, (1995).
21. Stott F H, Wei F I, Enahoro C A, *Mater Corros* **40** (1989) 198.